Scientific African 27 (2025) e02593

Contents lists available at ScienceDirect

Scientific African

journal homepage: www.elsevier.com/locate/sciaf

Statistical design for optimal physical and biomechanical characteristics of biocomposite prostheses

Ibrahim Hassan Kobe [a,c], Abdulrahman Asipital Salawu [b], Abolarin Mathew Sunday [a], Adedipe Oyewole [a], Okoro Gregory Uzoma [a], Peter Olorunleke Omoniyi [d,*], Tien-Chien Jen [d]

[a] Department of Mechanical Engineering, School of Infrastructure, Process, Engineering and Technology, Federal University of Technology, Minna, Niger State, Nigeria
[b] Department of Materials and Metallurgical Engineering, School of Infrastructure, Process, Engineering and Technology, Federal University of Technology, Minna, Niger State, Nigeria
[c] Department of Mechanical Engineering, Faculty of Engineering and Technology, University of Ilorin, Ilorin, Nigeria
[d] Department of Mechanical Engineering Science, University of Johannesburg, South Africa

ARTICLE INFO

Editor: DR B Gyampoh

Keywords:
Design, Biomechanical
Prosthesis
Optimisation
Biocomposite

ABSTRACT

The mechanical properties of many prostheses are the causes of the stress shielding effect resulting from the imbalance of the prosthesis and human bone, which leads to the premature failure of the prosthesis after installation for bone replacement or repair. The present study uses statistical design to obtain optimal biomechanical properties of biocomposite prostheses to replace orthopaedic bone. The study utilized Pure Titanium (P-Ti) powder reinforced with Hydroxyapatites (Ha) and Calcium Carbonate ($CaCO_3$) as the factors of the experiment, and the physical and mechanical properties were considered as the response. The experiment design was conducted with statistical software (Design Expert) using Determinant Optimal Mixture Design of Experiment (DM-DOE) and analyzed using analysis of variance (ANOVA). Biocomposites were developed using powder metallurgy techniques, and the experimental samples' mechanical, physical, and morphological characteristics were analyzed. The result showed that the optimum biocomposite formulations are 68.36 Ti, 18.36 Cow Bone-Based Hydroxyapatites (CB-Ha), and 8.17 $CaCO_3$ by maximizing the mechanical properties and minimizing stiffness and physical properties suitable for the replacement bone. The results revealed a closer value of bone modulus with the decreased modulus (54.23 GPa), density (4.09 g/cm^3), and porosity (9.56 %). There was also an enhancement of other mechanical properties with predicted compressive strength (162.17 MPa), Hardness (378.62 Hv), impact strength (11.43 KJ/m^2), and Fracture toughness (26.11 MPa m0.5). The ANOVA revealed that CB-Ha and $CaCO_3$ are crucial factors in minimizing the prosthesis stiffness, which has interactive effects on the formulation of biocomposite.

Introduction

Orthopedic implants are prostheses or devices for treating, repairing, and replacing bone atrophy [1]. The commonly used

* Corresponding author.
E-mail address: omoniyi.po@unilorin.edu.ng (P.O. Omoniyi).

https://doi.org/10.1016/j.sciaf.2025.e02593
Received 24 August 2024; Received in revised form 25 November 2024; Accepted 12 February 2025
Available online 12 February 2025

load-bearing implants are mainly manufactured from metallic (Stainless, Cobalt-chromium, Titanium) and alloys that are prone to corrosion attack, releasing toxic metallic ions into the body [2,3] and causing a stress distribution effect due to a variance in the modulus of the patient's bone with the implant [4].

It was reported that composite materials demonstrate the most helpful balance in strength, fracture toughness, fatigue, wear, and corrosion resistance [5]. Therefore, it is achievable to customise the properties of failing prostheses through the development of biocomposite as it is required in various medical applications by optimal combinations of matrix and reinforcement, with suitable fabricated design of materials [6]. Formulation of nano- Hydroxyapatites (Ha)/collagen, nano-Ha/polycaprolactone, and Ha/calcium sulphate biocomposite have been developed utilizing conventional methods to improve the rate at which new bone grows [7]. In this method, the total amount of all matrix and reinforcement constituents is identical to the American Concrete Institute (ACI) absolute volume approach, with fixed (mass or volume) and factors representing the proportions of the total quantity of mixture. Therefore, investigating the effects of the proportion of components in formulation requires a mixture of experimental designs. The conventional approach of mixture proportions and guidelines including the Rule of mixture, ACI 363–1997, United States Bureau of Reclamation (USBR), ACI 211.1(R2009), Indian standard (IS), and British Department of Environment (BDOE) that provide some approach for varying a given mixture of composites. It is typically performed in alloy and composite design by changing a single element at a time. Still, the procedures for finding the optimum mixture regarding the best performance with the least cost are not provided [8]. This provides the best components setting to achieve the required performance, but it cannot identify how variables interact and create prediction equations for further optimization. These approaches require huge experimentation to attain the desired attributes and make the procedure expensive, which brings about the utilization of computational methods. However, most computational methods are established on the principle of optimal design. Computer applications are necessary to develop the designs with software that can conveniently run and analyse the interaction, Contour Plot, 3D Response plot, and the effect of excipients, etc. Many software packages have statistical tools that are utilized for optimization or to develop an experimental design, including Multi-Simplex, Minitab, SAS, ECHIP, SYSTAT Software for general statistical nature, NEMRODW, GraphPad Prism, and Design Expert [9].

Many researchers have used the statistical mixture design approach where the non-negative component proportions adding up to one are the predictor factors for the production of concrete [8], biocomposite [10,11] nanocomposite [12] structures, coating materials [13,14], chemical, pharmaceutical, and biomedical products [15]. The composition and structure of a product with a heterogeneous distribution of qualities can be controlled by using combination rules that link essential properties to the product's composition by combining two or more biomaterials, including hybrid ceramics and metallic biomaterials. A sufficient mechanical performance of the final product is acquired by optimal designs including determinant (D), average variance (A), integrated variance (I), and Eigenvalue (E) optimality criteria for response function estimation [16]. D-optimal indicates the determinant design for 2–24 factors that minimize the proportion of the dependent parameters in a model since it is helpful for multiple constrained designs [17]. The D-optimal design can be modified for the study and offers maximum and determinant prediction power in a chosen group of experimental trials involving multiple biomaterials to develop biocomposites [17]. The study aims to utilize statistical design to obtain optimal biomechanical properties of biocomposite prostheses to replace orthopaedic bone.

Material and methods

Preparation and characterisation of the biomaterials

The biomaterials for this research include commercial Pure-Titanium (P-Ti), $CaCO_3$, and Ha. The P-Ti powder was acquired from Eternal Bliss Alloy Forging and Casting Co., China with approximately 45 μm particle size, 4.52 g/cm^3 density and chemical composition shown in Table 1.

The binder (Polyvinyl Alcohol), lubricant (Palm stearate), and medical grade $CaCO_3$ of the reinforcement biomaterial were acquired from a chemical shop located at the University of Ilorin Road, Tanke, Ilorin. The $CaCO_3$ was considered a biocompatible reinforcement biomaterial with purity and average particle size of 99 % (indicated by X-ray diffractometer) and 4.87 μm, respectively. Mature cow bones between the ages of two and six were acquired at the Ipata market in Ilorin, Kwara State, Nigeria, to produce the biomaterial from Cow Bone-Based Hydroxyapatite (CB-Ha). The process for obtaining CB-Ha biomaterials involves washing cow bones, degreasing, deproteinizing, oven-drying, calcining, and cooling in air, following Barua et al.'s [18] steps. A ball mill and sieve shaker were utilsed to grind the calcined bones into finer particles, achieving approximately 20 μm for the average grain size.

Optimization of biocomposite material compositions

The Design of Experiment (DOE) using Determinant Optimal Mixture Design of Experiment (DM-DOE) adopted for the statistical evaluation, Quality of Biocomposite by Design (QBD) considering the effects of biocomposite matrix and reinforcement fraction formulations on the physical and mechanical properties using Design-Expert package (version 8.0.6, Stat-Ease, Inc.). The mechanical

Table 1
Chemical composition of pure Titanium alloy.

Element	Ti	O	C	H	N	Fe
% composition	99.30	0.25	0.1	0.015	0.05	0.3

properties include compressive strength (DCS), modulus (DE), Hardness (DH), impact strength (DJc), and fracture toughness (DKc). The physical properties include porosity (DP) and density (Dρ). The ranges of P-Ti (50–94.5 vol%), CB-Ha, and $CaCO_3$ (0–45 vol%) and the mixture of constituents as the reinforcement components and the range of 0–20 % were used for space holder (Cp) material as considered in the previous studies [19,20]. The 3.9 vol% of binder (D), 0.2 vol% stabilizers (E), and 1 vol% of lubricant (F) were utilized, as considered by Srivabut et al. [21]. Table 1 shows the sample compositions, 100 % mixture, and the experimental design comprised 27 runs. The study considered five replications of samples, and the average outcome was calculated.

ANOVA and Response Surface Contour Model (RCM) analysis

The samples' overall formulation was optimized and analyzed using ANOVA and RCM. The impact of composition parameters on mechanical characteristics (impact strength, compressive strength, hardness, fracture toughness, and compressive modulus) and physical properties (Density and porosity) were assessed using the experimental data. The results for three test samples with a statistical significance level set at a 5 % level, and p-value <0.05 were statistically analyzed. Moreover, the mathematical model to fit the experimental data and responses for regression coefficients were generated using the quadratic model in Eq. (1), as Nooraziah and Tiagrajah [22] described. RCM was also utilized to find the interactions between three dependent factors of P-Ti, CB-Ha, and $CaCO_3$ and the responses.

$$Y = \sum_{i=1}^{k} \beta_i x_i + \sum \sum_{i<j}^{k} \beta_{ij} x_i x_j \quad (1)$$

where Y = response variables (hardness, impact strength, compressive modulus, fracture toughness, compressive strength, density and porosity properties); x_i = dependent factor, $x_i x_j$ = quadratic interaction coefficient of variables, b_{ij} and b_i are interaction terms and first-order coefficients, respectively.

Production of experimental specimens

The Dense Structure Biocomposite (DSB) samples were fabricated using the powder metallurgy technique based on formulation compositions stated in Table 2 generated from the design mixture of experimental data. A Jar mixer was used to blend the powdered biomaterials for 20 mins. The mixed powder was filled into the constructed cylindrical die (30 mm of external diameter, 10 mm of internal diameter, and 20 mm of height). The mixtures were compressed uniaxially for 30 mins at 400 MPa of pressure using an electrically powered hydraulic press (WEIBER P100HE). Arifin et al. [23] described that the compressed material was removed to

Table 2
Constituent Formulations of DSB samples with DM-DOE and responses (Mechanical and Physical Properties).

Mixture Components							Responses						
Run	P-Ti %	CB-Ha %	$CaCO_3$ %	D %	E %	F %	DCS MPa	DE GPa	DH Hv	DJc KJ/m^2	DKc MPa(m^0.5)	Dp g/cm^3	DP %
1	59.98	25.2	9.72	3.9	0.2	1	146.17	46.72	363	10.3	22.99	4.14	8.41
2	50	41.3	3.6	3.9	0.2	1	135.47	36.62	402	9.8	19.86	3.93	13.05
3	92.07	0	2.83	3.9	0.2	1	368	76	388	18.7	39.52	4.21	6.86
4	60.6	14.3	20	3.9	0.2	1	142.23	42.83	365	11.8	23.57	3.92	13.27
5	50	25.69	19.21	3.9	0.2	1	136.76	37.21	405	9.5	19.71	3.96	12.39
6	69.11	15.28	10.51	3.9	0.2	1	167.65	53.74	391	11.1	25.60	4.05	10.40
7	74.9	0	20	3.9	0.2	1	192.22	64.22	372	14.5	31.99	4.17	7.74
8	94.9	0	0	3.9	0.2	1	437	87.26	357	23.7	47.67	4.37	3.32
9	50	25.69	19.21	3.9	0.2	1	136.76	37.21	405	9.5	19.71	3.96	12.39
10	74.9	0	20	3.9	0.2	1	192.22	64.22	372	14.5	31.99	4.17	7.74
11	80.15	14.29	0.46	3.9	0.2	1	224.1	72.15	352	17.7	37.46	4.29	5.09
12	69.11	15.28	10.51	3.9	0.2	1	167.65	53.74	391	11.1	25.60	4.05	10.40
13	59.98	25.2	9.72	3.9	0.2	1	146.17	46.72	363	10.3	22.99	4.14	8.41
14	69.11	15.28	10.51	3.9	0.2	1	167.65	53.74	391	11.1	25.60	4.05	10.40
15	70.66	24.24	0	3.9	0.2	1	198.34	65.31	368	14.5	32.26	4.24	6.20
16	92.07	0	2.83	3.9	0.2	1	368	76	388	18.7	39.52	4.21	6.86
17	60.85	34.05	0	3.9	0.2	1	158.23	48.33	395	12.7	25.97	4.11	9.07
18	69.11	15.28	10.51	3.9	0.2	1	167.65	53.74	391	11.1	25.60	4.05	10.40
19	70.66	24.24	0	3.9	0.2	1	198.34	65.31	368	14.5	32.26	4.24	6.20
20	94.9	0	0	3.9	0.2	1	437	87.26	357	23.7	47.67	4.37	3.32
21	69.11	15.28	10.51	3.9	0.2	1	167.65	53.74	391	11.1	25.60	4.05	10.40
22	81.45	4.66	8.79	3.9	0.2	1	210.15	68.25	345	16.5	35.18	4.09	9.51
23	50	41.3	3.6	3.9	0.2	1	135.47	35.62	402	8.8	18.56	3.93	13.05
24	92.07	0	2.83	3.9	0.2	1	368	76	388	18.7	39.52	4.21	6.86
25	50	41.3	3.6	3.9	0.2	1	135.47	36.62	402	9.8	19.86	3.93	13.05
26	50	25.69	19.21	3.9	0.2	1	136.76	37.21	405	9.5	19.71	3.96	12.40
27	70.66	24.24	0	3.9	0.2	1	198.34	65.31	368	14.5	32.26	4.24	6.20

produce unsintered biocomposite and heated between 200 and 500 °C to remove the binder and lubricant. The top punch for the hydraulic press and the wall of the die mold were adequately lubricated to avoid specimen bonding during ejection. The samples were consecutively cleaned in deionized water containing several drops of acetone to remove impurities. The heated green biocomposite specimens were sintered as conducted by Cummings et al. [24] and Shimp [25] under sintering temperatures of 800 °C for two hours in Murfle Furnance at a 10 °C/min heating rate.

Determination of morphological, physical, and mechanical properties

Morphological properties

The scanning electron microscope (SEM) and X-ray diffractometer (XRD) were utilized to determine the phase and morphological analysis of DSB following the ASTM F1185–03 standard for surgical implants.

Physical properties

The density and porosity of the sintered specimens were determined following the ASTM B962 standard using the mathematical expressions in Eqs. (2) and 3 [19,26] as follows;

$$\rho = \frac{m_D \rho_{water}}{(m_s - m_w)} \tag{2}$$

$$P = \left(\frac{m_w - m_D}{m_w - m_s}\right) X\ 100 \tag{3}$$

Each mass was determined three times for accuracy, and the mean values were used to determine the samples' bulk density (ρ) and porosity (P). Eqs. (2) and 3 were used to determine the porosity and bulk density, respectively. The density of sintered biocomposites was measured using the standard Archimedes' (water immersion) method:

m_D = dry mass, m_w = water-saturated mass, m_s = suspended mass

Mechanical properties

Compressive strength

UTM Testometric FS5080, of 100KN capacity (DBBMTCL-5000 Kg, Serial No 38,140, Rochdale, England), was used to conduct the compression test in accordance with ASTM 3039–79 standard. The specimens were prepared to a standard dimension of 20 mm diameter and 15 mm height to conform to the instrument's specification. The testing apparatus with two grips held each test sample firmly while gradually increasing the load at a constant value., as conducted in previous research [27]. Three specimens were tested, with loads and deflections recorded. The average results were computed till ruptured of the samples. Eqs. (4) and 5 were used to calculate the compressive strength, and total surface area, respectively from Li and Zhou [28] and Abutu et al. [29].

$$Compressive\ Strenght\ (CS) = \frac{Max.\ Applied\ Load\ (AL)}{Total\ Crossectional\ Area\ (TCA)}\ (MPa) \tag{4}$$

$$Total\ Crossectional\ Area\ (TCA) = \pi r^2 h \tag{5}$$

Determination of hardness value

The hardness of the samples was conducted with ASTM E-92 standard using Digital Micro Vickers Hardness Tester (HVC-30E). The specimen dimension of the tester is 3.142 × 20ˆ2 × 10 $mm^{2,}$ as Sadashiva et al. [30] demonstrated. The sample was mounted on a stage clamp, and microscopic measurements were conducted using a low objective, selecting an area below the pyramidal diamond indenter. The microscope measurement objective was reattached to the sample-holding stage clamp, and the 2 kg weight was released after gradual application and 15-second holding.

Determination of impact strength and fracture toughness

The impact strength test was conducted using a Charpy impact testing apparatus with a 150J/300 J capacity, 2 Joules of minimum scale gradation and model No of 6705U/33,122, Leeds, LS102DE England. The machine has specifications such as a pendulum weight

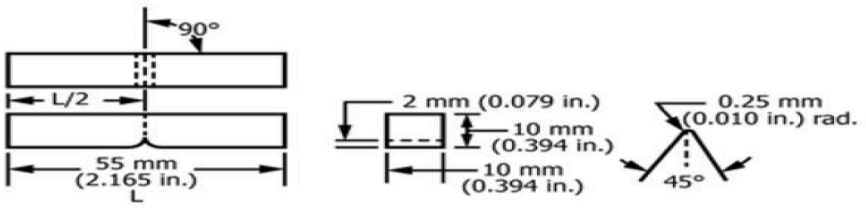

Fig. 1. Standard specimen schematic with dimension (Source: [31]).

of 21.79 Kg, a striking energy of 168 N-m or Joules, and a permissible total friction loss of 0.50 %. The specimens were machined in compliance with ASTM E23 testing procedures with 55 × 10 × 10 mm specimen size, has a 0.25 mm radius along the base, 2 mm depth and 45-degree notch angle as depicted in Fig. 1 [31]. The specimen was placed across the machine's jaws, and the pendulum hammer was released downwards. The broken specimens were removed by loosening the clamping screw, and the actual energy absorbed by fractured specimens (E_a) was determined using Eq. (6).

$$E_a = E - E_f \tag{6}$$

The specimens' impact strength (J_c) was determined using Eq. (7) [32].

$$J_C = \frac{Energy\ in\ Fracture\ (E_a)}{Crosssectional\ Area\ at\ Notch\ (CA)} \left(\mathrm{KJ}/\mathrm{m}^2\right) \tag{7}$$

The fracture toughness (K_C) was calculated from the expression that links the impact strength (energy release rate) J_c in (KJ/m^2) with other properties of materials (modulus and poison ratio) [33,34] in Eq. (8), following ASTM E1820–08 standard:

$$K_C = \sqrt{\frac{J_C \cdot E}{1-\nu^2}} \tag{8}$$

Results and discussion

Statistical design for optimal biomechanical properties of biocomposites

The biocomposite samples were produced, as shown in Fig. 2. The samples were used to conduct different physical and mechanical properties tests to examine the interaction and relationship between design factors. The effects of mixture proportions on the responses to the physical and mechanical properties of the biocomposites are displayed in Table 1. The data underwent statistical analysis to validate model variables and establish mathematical functional linkages using Software (Design Expert). A quadratic model was found to fit adequately the experimental data.

Fitting of models and Anova Analysis for DSB

The results of P-values <0.05 are utilized in additional examination of the results from ANOVA analysis, a statistical model used to assess the significance of response models. This experimental work determined factors for optimal composition by using P-Ti, CB-Ha, $CaCO_3$, Binder (PVA), stabilizer, and Lubricant (Palm stearin). The response models presented for mechanical and physical properties were analyzed using the quadratic models. The summary of the best-fitting model for biomechanical properties with the quadratic model is presented in Table 3. The fitted model of the dense biocomposite compressive strength attribute shows that the sequential model sum of squares for a quadratic model value of <0.0001 is significant ($p < 0.05$) as shown in Table 4. The adjusted R^2 was found to be 0.9811 and 0.9950, while the predicted R^2 values of 0.9770 and 0.9730 were also suggested for DCS, indicating a well performance with the significance of the model. The quadratic model values of 0.0127, with a sequential model sum of the square, are significant ($p < 0.05$) in the DE property model as shown in Table 5. Furthermore, The corrected R^2 value is 0.9843, with a predicted R^2 value of 0.8387 for dense biocomposite modulus (DE). The lack-of-fit value for the quadratic model is negligible. These results indicated the model that is significance and performed well. The results obtained matched with the experimental findings of Homkhiew et al. [35] and Srivabut et al. [21].

The ANOVA results of dense structure biocomposites for each biomechanical and physical properties were presented in Table 5, showing the quadratic models for ANOVA analysis based on the experimental findings. The model's substantial compressive strength and modulus are indicated by F-values of 271.02, 210.74, and 22.52, with noise potential 0.01 % cases. Model terms are significant when P-values are <0.0500, and model reduction enhances it (Alsaiari et al., 2022). The ANOVA demonstrated the statistical significance of the terms complementing linear models for all responses, indicating an acceptable value as shown in Tables 6–7. This reveals the significant interactions with response models, especially in the case of P-Ti, CB-Ha, and $CaCO_3$ for all mechanical properties and density. However, the low F-value indicated $CaCO_3$ material porosity with no interactions between P-Ti, especially at temperatures

Fig. 2. Experimental samples for conducting mechanical and physical properties of biocomposites.

Table 3
Summary of fitted model for DSB compressive strength.

Biocomposites	Source	Sequential p-value	Adjusted R^2	Predicted R^2	
DCS					
	Linear	< 0.0001	0.8082	0.7705	
	Quadratic	**< 0.0001**	**0.9811**	**0.9770**	**Suggested**
	Special Cubic	0.0174	0.9852	0.9703	
	Cubic	**< 0.0001**	**0.9950**	**0.9730**	**Suggested**
	Sp Quartic vs Quadratic	0.0010	0.9909	0.5816	
	Quartic vs Cubic		1.0000		**Aliased**
	Quartic vs Sp Quartic		1.0000		Aliased

Table 4
Summary of fitted model for DSB compressive modulus.

Biocomposites	Source	Sequential p-value	Lack of Fit P-value	Adjusted R^2	Predicted R^2	
DE						
	Linear	< 0.0001	< 0.0001	0.9529	0.9440	
	Quadratic	0.0007	< 0.0001	0.9758	0.9675	
	Special Cubic	0.0645	< 0.0001	0.9787	0.9599	
	Cubic	< 0.0001	< 0.0001	0.9946	0.9486	
	Sp Quartic vs Quadratic	**0.0127**	**< 0.0001**	**0.9843**	**0.8387**	**Suggested**
	Quartic vs Cubic	< 0.0001		0.9998		**Aliased**
	Quartic vs Sp Quartic	< 0.0001		0.9998		Aliased

Table 5
ANOVA results for DSB compressive strength.

Biocomposites	Source	Sum of Squares	Df	Mean Square	F-value	p-value	
DCS							
	Model	2.327E+05	5	46,538.77	271.02	< 0.0001	significant
	Linear Mixture	1.945E+05	2	97,234.70	566.25	< 0.0001	
	AB	17,021.02	1	17,021.02	99.12	< 0.0001	
	AC	4805.00	1	4805.00	27.98	< 0.0001	
	BC	509.15	1	509.15	2.97	0.0998	
	Residual	3606.03	21	171.72			
	Lack of Fit	3606.03	6	601.01			
	Pure Error	0.0000	15	0.0000			
	Cor Total	2.363E+05	26				

above 800 °C, leaving some structures with pores [25]. The presence of pores in the biocomposite contributed to reducing the compressive strength and modulus. Other ANOVA results for hardness, fracture toughness, impact strength, and density are significant. The compressive strength's Lack of Fit F-value of 480.01 is significant, with only a 0.01 % chance of noise causing such a large F-value while others show an negligible lack of fit.

Additionally, the ANOVA analysis assessed the performance of the developed response model using fit statistics such as coefficients of determination, adjusted R^2, predicted R^2, adequate precision, mean standard deviation, and coefficients of variation., as given in Table 8. For example, the quadratic model of the biocomposite properties shown had a significant coefficient of determination with a higher value of R^2 than 0.9704, except for the dense biocomposite hardness (0.4611). The R^2 for each response indicated a strong correlation between process variables and the characteristics of composite samples [36]. The Predicted R^2 of the biocomposite samples

Table 6
ANOVA results for DSB compressive modulus.

Biocomposites	Source	Sum of Squares	df	Mean Square	F-value	p-value	
DE							
	Model	6456.19	5	1291.24	210.74	< 0.0001	significant
	Linear Mixture	6298.55	2	3149.28	513.99	< 0.0001	
	AB	34.20	1	34.20	5.58	0.0279	
	AC	128.04	1	128.04	20.90	0.0002	
	BC	119.95	1	119.95	19.58	0.0002	
	Residual	128.67	21	6.13			
	Lack of Fit	128.00	6	21.33	480.01	< 0.0001	significant
	Pure Error	0.6667	15	0.0444			
	Cor Total	6584.86	26				

Table 7
ANOVA results for DSB biocomposite porosity.

Biocomposites	Source	Sum of Squares	df	Mean Square	F-value	p-value	
DP							
	Model	196.50	5	39.30	22.52	< 0.0001	significant
	Linear Mixture	171.36	2	85.68	49.10	< 0.0001	
	AB	10.60	1	10.60	6.08	0.0224	
	AC	16.92	1	16.92	9.70	0.0053	
	BC	13.45	1	13.45	7.71	0.0113	
	Residual	36.65	21	1.75			
	Lack of Fit	36.65	6	6.11			
	Pure Error	0.0000	15	0.0000			
	Cor Total	233.14	26				

is in reasonable agreement with the Adjusted R^2, which revealed the difference is <0.2. Adeq Precision measures the signal-to-noise ratio. A ratio greater than 4 is desirable [29]. Table 8 also shows the Adeq Precision results with an adequate signal and desirable model, which can be utilized to navigate the design space effectively.

The experimental results showed good fits and reliability with R^2 values in the 0.4611–0.9847 range, while the adjusted R^2 of regression analysis ranged from 0.3328 to 0.9764 as revealed in Table 8. Regression analysis utilizes the predicted R^2 to evaluate the model's ability to accurately predict response models for new observations [37]. The biocomposite compressive strength model accounts for 97.70 % of fresh term data variability, with coefficients of variation (CV) ranging from 1.45 to 14.66 %. Residual variation should not exceed 15 % [38], with the obtained lowest CV of 1.45 % for dense biocomposite density, indicating the experimental results' highest reliability and degree of precision. However, the biocomposite porosity has the highest CV (14.66 %), indicating better precision closer to 15 %, which could be attributed to the pore generation and decreasing biocomposite modulus as one of the beneficial properties of reducing stress shielding effect.

Diagnostic verification of the models

The models were tested using diagnostic charts, including normal probability, expected response, and predicted response vs actual values as shown in Fig. 3–5. Meanwhile, a strong fit is necessary for accurate results. However, observation of the fitted response surface model may produce poor or misleading results unless the model shows a good fit, which is essential to check the model's adequacy [21]. Figs. 3 and 4 depict the normal probability plot of residuals, or the normal plot distribution of residuals for response models.

The residuals and run response plots reveal linear patterns in experimental values, normal distribution of response, and random scatter residuals. It can be observed in Fig. 4 that one of the experimental runs was out of the residual control, and this is attributed to an experimental error during the experimental analysis [39]. Finally, Fig. 5 shows actual data and projected response plots, with no issues found in odelled responses. Expected reactions closely matched experiment outcomes, with sufficient agreement between expected and actual values.

Optimization and effects of compositions on biomechanical properties

Optimization and effects of compositions on compressive strength properties

ANOVA analyzed the data of each response, and these constituents were optimized using the response contour model (RCM) method. The compressive modulus and strength of DSB samples gradually decreased with an increased proportion of reinforced bioceramics (CB-Ha and $CaCO_3$) in the P-Ti matrix. Such a decrease in the modulus results is consistent with the compressive strength and modulus obtained by Yılmaz et al. [40] and Xie et al. [41]. The quadratic models provided regression equations to predict the effects of compositions on compressive strength and modulus of both DSB:

$$DCS = +4.4324P\text{-}Ti + 5.9573CB\text{-}Ha + 17.3972CaCO_3 - 0.1534(P\text{-}Ti * CB\text{-}Ha) - 0.327\ (P\text{-}Ti * CaCO_3) - 0.1115(CB\text{-}Ha * CaCO_3) \quad (9)$$

$$DE = +0.8916P\text{-}Ti - 0.4514CB\text{-}Ha + 3.7875CaCO_3 + 0.0069(P\text{-}Ti * CB\text{-}Ha) - 0.0535(P\text{-}Ti * CaCO_3) - 0.0541(CB\text{-}Ha * CaCO_3) \quad (10)$$

Table 8
Fit statistic results for DSB biocomposites properties.

Properties	Std. Dev	Mean	C.V %	R^2	Adjusted R^2	Predicted R^2	Adeq. Precision
DCS	34.94	208.87	6.27	0.9847	0.9152	0.9770	46.2620
DE	2.48	57.08	4.34	0.9805	0.9758	0.9675	41.5803
DH	14.99	380.93	3.94	0.4611	0.3328	0.2215	5.5962
DJc	0.8140	13.62	5.98	0.9704	0.9634	0.9541	33.8885
DKc	1.31	29.19	4.49	0.9809	0.9764	0.9701	42.6589
Dp	0.0597	4.11	1.45	0.8428	0.8054	0.7492	13.2444
DP	1.32	9.01	14.66	0.8428	0.8054	0.7492	13.2444

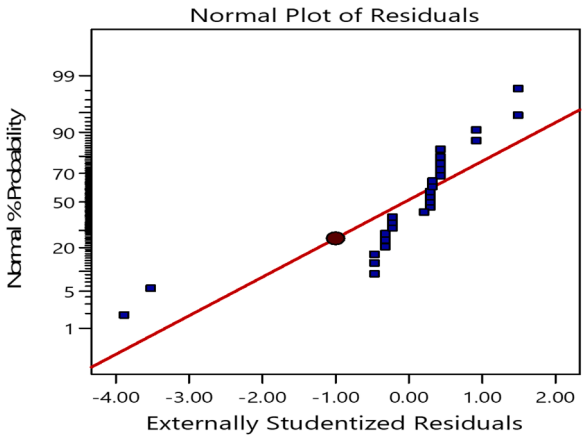

Fig. 3. Normal plot of residuals for dense biocomposite compressive strengths.

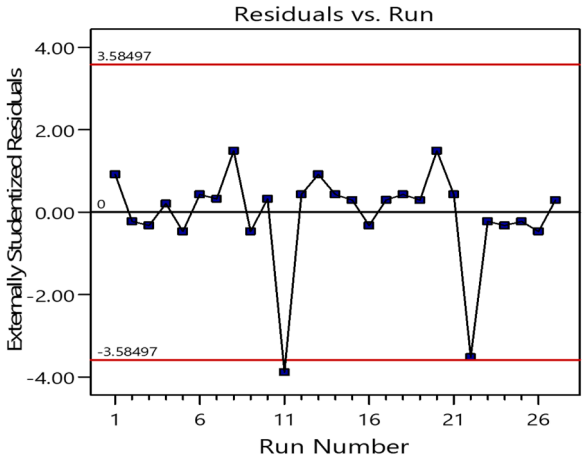

Fig. 4. Residuals vs. run for dense biocomposite compressive strengths.

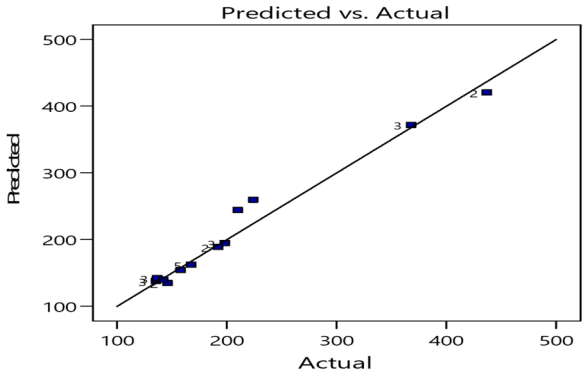

Fig. 5. Predicted vs. actual of dense biocomposite compressive strengths.

The extended quadratic model reveals a correlation between the factors P-Ti, CB-Ha, and $CaCO_3$ and the compressive strength response, as illustrated in Eqs. (9) and (10). The R^2 values of 0.9847 and 0.9805 for compressive strength and modulus response models respectively were obtained which referred to the good fits and reliability of the experimental results. Compressive strength and modulus response regression equations display negative coefficients for main effects and positive coefficients for interaction terms. It was observed that the interaction between matrix (P-Ti) and other bioceramics (CB-Ha and $CaCO_3$) shows negative coefficients for

both dense biocomposites with porosity. The reactions between the three components also resulted in significantly negative coefficients due to the biocomposite values' decreasing compressive strength and modulus with increased bioceramics. Figs. 6–7 in DSB display the response model's contour plots for modulus and compressive strength. The av'rage compressive strength responses of dense biocomposite samples ranged from 135.47 MPa to 437 MPa and 35.62 GPa to 87.26 GPa for compressive modulus. These values fall within the acceptable strength and stiffness of cortical as established in the literature [42,43] except in the range of higher modulus for dense biocomposite which is also closer to the modulus of bone (10–30 GPa) compare to standard titanium implant that has modulus in the range of 100–110 GPa (Petersen 2014).

The compressive strength and modulus decreased with the ideal amount of $CaCO_3$ (ranging from 0 to 20 vol%). This is because it creates pores in dense biocomposite structures, reducing the stiffness properties of the biocomposites without affecting their strength. The compositions in Figs. 6 and 7 display compressive properties that increase with the increasing P-Ti and decrease with increasing reinforced bioceramics. Moreover, The expected response values for compressive strength and modulus were 162.171 MPa and 54.23 GPa, respectively, as shown in Fig. 8. The optimal formulation for dense biocomposite was achieved with a desirability score value of 0.3441 for dense biocomposite.

Optimization and effects of compositions on hardness properties

The quadratic model displayed the highest hardness attributes, allowing the determination of the mean regression equation for dense biocomposites as I Eq. (11):

$$DH = +3.9028P\text{-}Ti + 6.4419CB\text{-}Ha - 0.2656CaCO_3 - 0.03776(P\text{-}Ti * CB\text{-}Ha) + 0.0571(P\text{-}Ti * CaCO_3) + 0.0746\ (CB\text{-}Ha * CaCO_3) \quad (11)$$

The biocomposite sample models have an R^2 of 0.4611, as indicated by Eqs. (11) and the regression analysis of the answers reveals correlation coefficients. As seen from both equations, the negative coefficients of $CaCO_3$ are highest in the model fits, with values of 0.2656. This was due to the increased interfacial adhesion with the presence of $CaCO_3$, which has been considered a binder [44] or cementing material [45] that resulted in the improved hardness properties of biocomposite samples. The optimal hardness was obtained with loading 18.36 CB-Ha and 8.18 $CaCO_3$ vol% for dense biocomposite. The study found that bioceramic components can alter their mechanical and physical properties by enhancing contact and altering micro-morphology [46]. Moreover, the predicted hardness value is 378.625 Hv. The compositions for various hardness qualities matched the research findings [47], maximizing responses based on their order of priority.

Optimization and effects of compositions on the impact strength and fracture toughness

The impact strength and fracture toughness values of biocomposite samples were fit in quadratic regression models with equations for DSB samples shown in Eqs. (12) and 13:

$$DJc = +0.2363P\text{-}Ti + 0.1254CB\text{-}Ha + 1.91778CaCO_3 - 0.0029\ (P\text{-}Ti * CB\text{-}Ha) - 0.0278\ (P\text{-}Ti * CaCO_3) - 0.0240\ (CB\text{-}Ha * CaCO_3) \quad (12)$$

$$DKc = +0.4814P\text{-}Ti + 0.0204CB\text{-}Ha + 3.0350CaCO_3 - 0.0013(P\text{-}Ti * CB\text{-}Ha) - 0.0435(P\text{-}Ti * CaCO_3) - 0.0397(CB\text{-}Ha * CaCO_3) \quad (13)$$

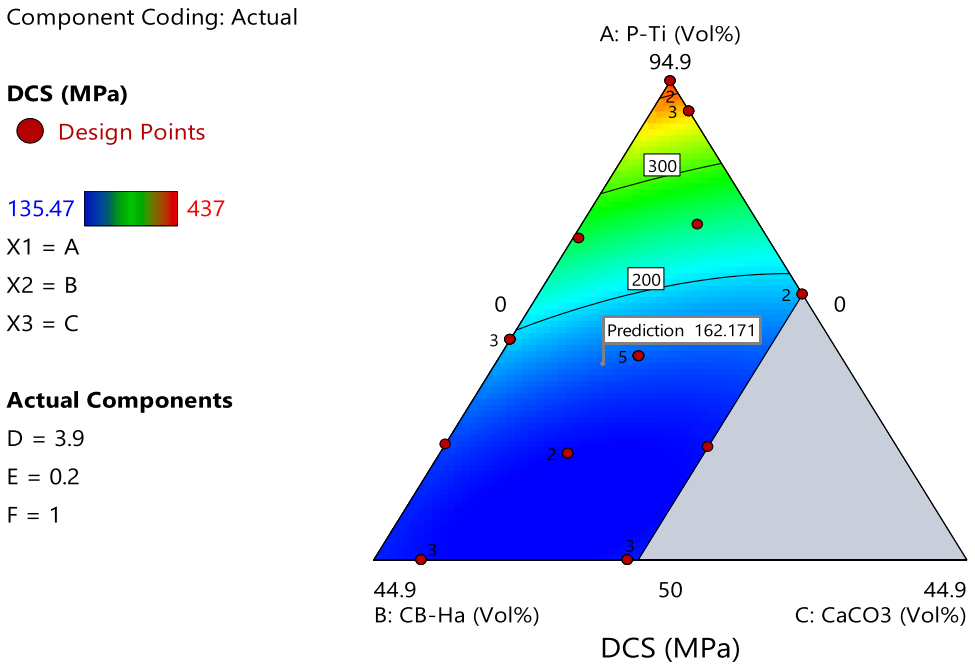

Fig. 6. Contour plot for compressive strength of dense biocomposite.

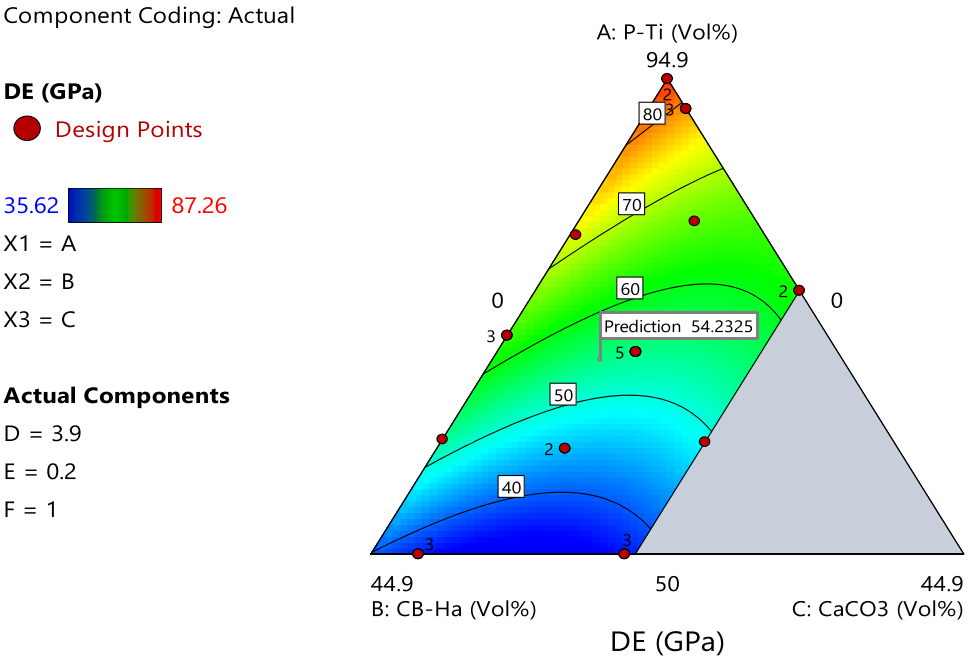

Fig. 7. Contour plot for compressive modulus of dense biocomposite.

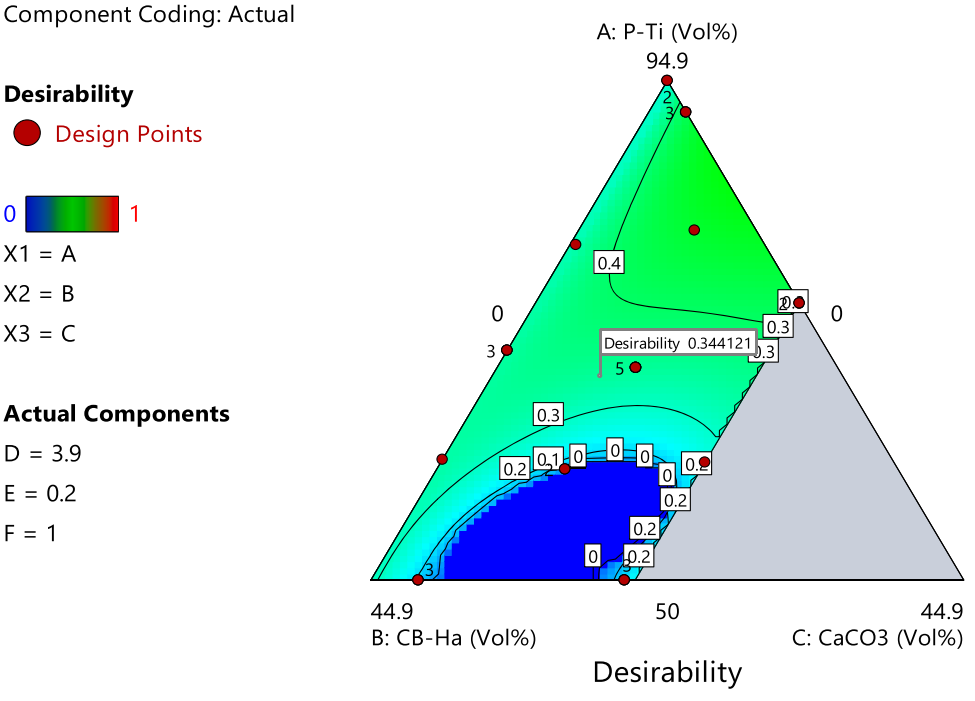

Fig. 8. Desirability contour for dense biocomposite.

It can be observed that most of the factors in the equations show positive coefficients for the P-Ti and bioceramics (CB-Ha and $CaCO_3$) factors, and the highest negative coefficient was due to the interaction of bioceramics that resulted in burn-off $CaCO_3$ at a very high temperature during sintering, significantly affecting the response models. This may be attributed to the reinforced bioceramic ($CaCO_3$) material that contributes to the porosity of biocomposite by losing carbonate in the form of CO_2 at higher sintering temperatures above 800 °C [24]. As a result, 11.4289 KJ/m^2 and 26.1079 MPam0.5 were obtained from RCM, respectively, as predicted impact strength and fracture toughness. The R^2 values of 0.9704 and 0.9809 for impact strength and fracture toughness response

models respectively were obtained which referred to the good fits and reliability of the experimental results The impact strength appears closer to the 6 KJ/m^2 value of bone impact strength [48]. The responses increased with the increase in P-Ti since the impact energy could result in premature fracture or sudden failure of the samples with low metal powder content in the composites' development, making them dimensionally unstable for orthopedic applications [49].

Optimization and effects of compositions on density and porosity properties

The density (p) and porosity (P) are some of the most critical biocomposite samples attributes exposed to physiological environments and conditions where they can be applicable in the body system. The responses minimize the density and maximize porosity values. It has been established that lowering the sintering temperature leads to decreasing biocomposite density and increasing the porosity of biocomposites [25]. The most appropriate way to express the regression model based on the responses was with quadratic models in Eqs. (14) and 15 as follows:

$$Dp = +0.0455\ \text{P-Ti} + 0.0298\ \text{CB-Ha} + 0.1011\ CaCO_3 + 0.0001\ (\text{P-Ti} * \text{CB-Ha}) - 0.0009\ (\text{P-Ti} * CaCO_3) - 0.0008\ (\text{CB-Ha} * CaCO_3) \quad (14)$$

$$DP = +0.0467\ \text{P-Ti} + 0.3949\ \text{CB-Ha} - 1.1820\ CaCO_3 - 0.0038\ (\text{P-Ti} * \text{CB-Ha}) + 0.0195\ (\text{P-Ti} * CaCO_3) + 0.0181\ (\text{CB-Ha} * CaCO_3) \quad (15)$$

The equation models of density and porosity display positive coefficients for all factors except $CaCO_3$ interaction, with the highest negative coefficients of 1.1820 $CaCO_3$ vol% contributing to the porosity properties of biocomposites. Therefore, the porosity increased with increasing $CaCO_3$. This may result from the higher sintering temperature that burns off $CaCO_3$ above 800 °C, losing carbonate in the form of evolving CO_2 gas, leading to pore development in the biocomposites [50]. Figs. 9 and 10 display contour graphs of density and porosity properties from response models. These triangular plots show the dense biocomposite's best response prediction values and the three-factor compositions (P-Ti, CB-Ha, and CaCO3) with R^2 values of 0.8428 indicating a good fit. Also, the best density and porosity predicted values of 4.0877 g/cm^3 and 9.4643 were obtained for the dense biocomposite, respectively. These findings corroborate the experimental density and equivalent porosity obtained in the literature [4,51].

Optimization of overall biomechanical and physical properties of biocomposite

The desirability score balances fitted models, revealing composite compositions as most effective. Fig. 11 shows response surface contours and ideal compositions of total desirability score.

This formulation of the biocomposite samples was used to select the most suitable implant for orthopedic applications. Table 9 presents a comparison of the experimental outcomes with each ideal formulation.

The microstructure of the DSB was examined using SEM analysis and pore distribution analysis from Image J software, as shown in Fig. 12. High sintering temperatures caused scratches in the biocomposite microstructure due to $CaCO_3$ response, releasing CO_2 and causing pores to grow on the surface [50]. The findings confirmed on Image J software validated the result of the porosity from the predicted porosity from optimization and the experimental porosity. The measured porosities contributed to the closeness of the modulus to the cortical bone modulus, which prevents bone resorption resulting from stress shielding [52]. Furthermore, It has been reported that the surface roughness properties play important roles in the stability of an implant in which rough implant surface favours both biomechanical stability and bone anchoring using surface roughness parameters, i.e., average roughness (Ra), root-mean-square roughness (Rq) and maximum profile height (Rt) [53]. The surface roughness results of DSB obtained from ImageJ software are shown in Fig. 13 for the roughness surface plot (A) and the profile plot (B) with surface roughness parameters of 14.2809 μm, 20. 0502 μm and 194.925 μm for R_a, R_q and R_t respectively. Jurczyk et al. [54] reported low surface roughness parameters for the bulk Ti–10 wt.% 45S5 Bioglass nanocomposite (R_a = 0.91 μm, R_q = 10.21 μm and R_t = 12.99 μm) and higher Ti–10 wt.% 45S5 Bio-glass scaffold with 67 % porosity (R_a = 54 μm, R_q = 392 μm and R_t = 405 μm) confirming the surface roughness of DSB which is due to the presence of $CaCO_3$ which releasing CO_2 at high sintering temperatures caused scratches and create pores in the biocomposite microstructure. However, the XRD result confirmed the DSB is crystalline and amorphous with important compounds, as shown in Fig. 14.

The sharp peak intensity peaks were observed in XRD patterns shown in Fig. 14, confirming the complete crystallization of the DSB specimen after the biocomposite sintered at 800 °C. The titanium peak could be observed as the major peak, with some other new phases being discovered, including TCP, TTCP, CaO, $CaTiO_3$, and traces of TiO_2. The formation of the phases resulted from the decomposition that occurred during the interaction of the titanium matrix and the reinforcement (CB-Ha and $CaCO_3$) in the biocomposite. Arifin et al. found that Ti/HA composites interact at 700 and 1200 °C, creating TiO_2 at 800 °C in two crystalline phases: Calcium titanate ($CaTiO_3$) and TiO_2. The interaction between titanium and HA produces $CaTiO_3$. Similar phases were confirmed in other studies by Choy et al. [50], Qian et al. [42], and Zakaria et al., [19] which revealed the phases have no adverse effect on the biocompatibility of the biocomposite, which has been established to be an osteoconductive material with good biocompatibility that is suitable for the promotion of new bone formation and use in implant applications.

Conclusion

This research developed different structure biocomposite implants with P-Ti, CB-Ha, and $CaCO_3$ biomaterials powder metallurgy techniques. The biomaterials were characterized with various examinations specified in ASTM standards for investigating biomaterial particles. The developed biocomposites were optimized to study the effect of biomaterials on the biomechanical and physical properties using DM-DOE. From the results, the following conclusions are drawn. The ANOVA results provided valuable insights into the

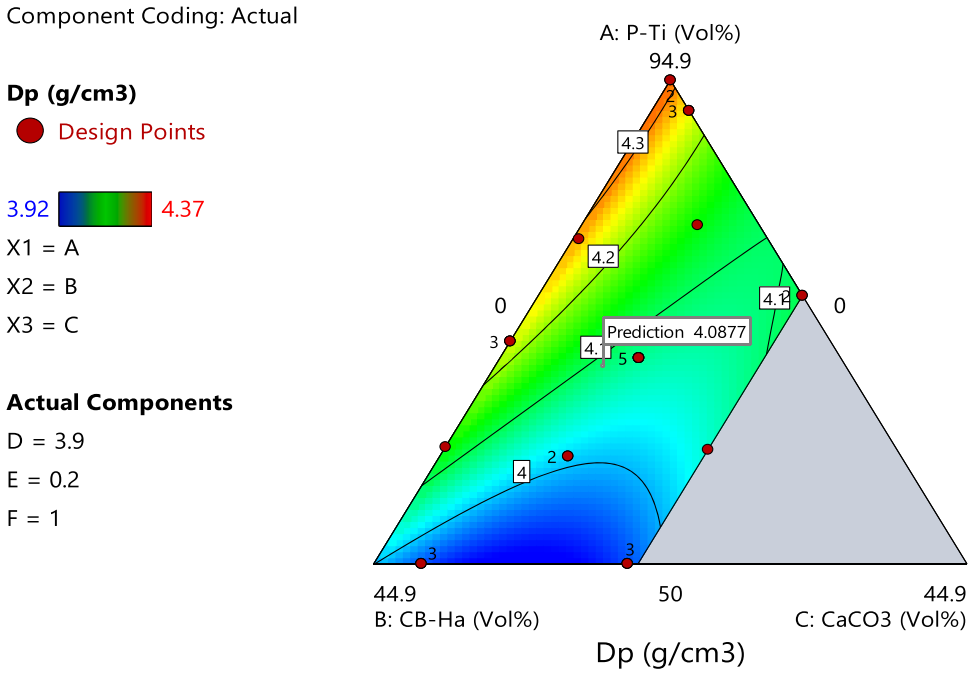

Fig. 9. Density response contour model for dense biocomposite.

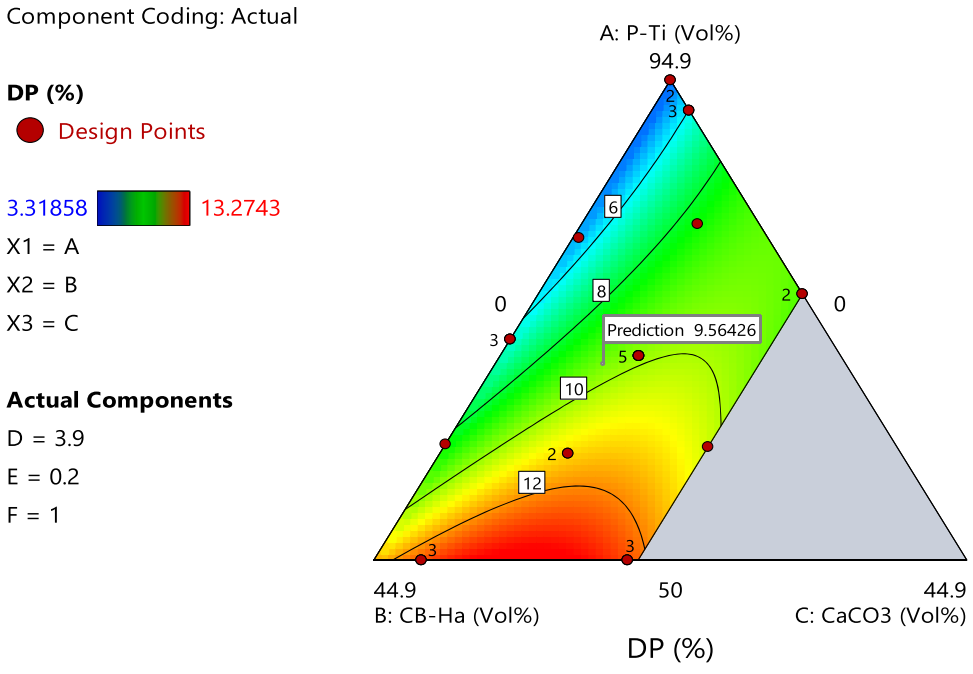

Fig. 10. Porosity response contour model for dense biocomposite.

individual and interactive effects of the formulation variables, enabling the identification of key factors influencing the response variables. The RCM analysis further revealed the relationship between the formulation and response variables, allowing the prediction and optimization of biocomposite properties within the experimental design space. This approach facilitated the development of robust and optimum biocomposite formulations of DSB (68.36 Ti, 18.36 CB-Ha, 8.17 $CaCO_3$) with maximized mechanical properties. It minimizes stiffness and physical properties that are suitable for replacement bone. The results revealed a closer value of bone modulus with the decreased modulus (54.23 GPa), density (4.09 g/cm^3), and porosity (9.56 %). It also enhances the other mechanical properties with predicted compressive strength (162.17 MPa), Hardness (378.62 Hv), impact strength (11.43 KJ/m^2), and Fracture toughness

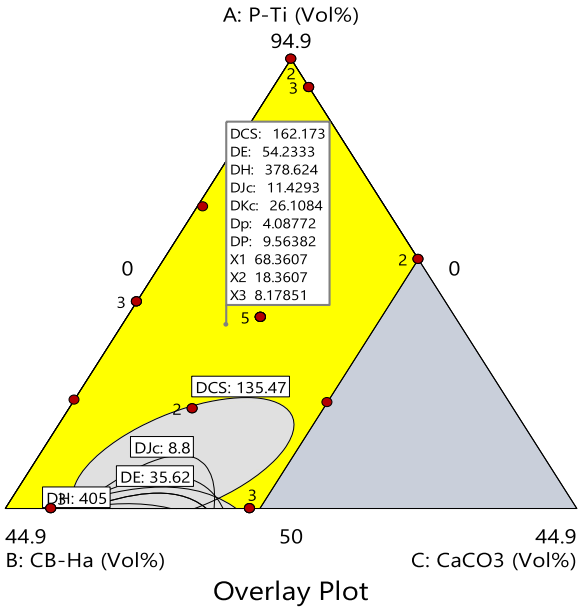

Fig. 11. Overlay plot for the dense biocomposites.

Table 9
The predicted and experimental results for biomechanical and physical properties.

Properties	DSB Predicted Values	DSB Experimental Values
CS (MPa)	162.17	164.23
E (GPa)	54.23	55.72
H (Hv)	378.62	377.14
Jc (KJ/m^2)	11.43	15.45
Kc (MPam$^{0.5}$)	26.108	27.23
p (g/cm^3)	4.087	4.03
P (%)	9.56	9.21

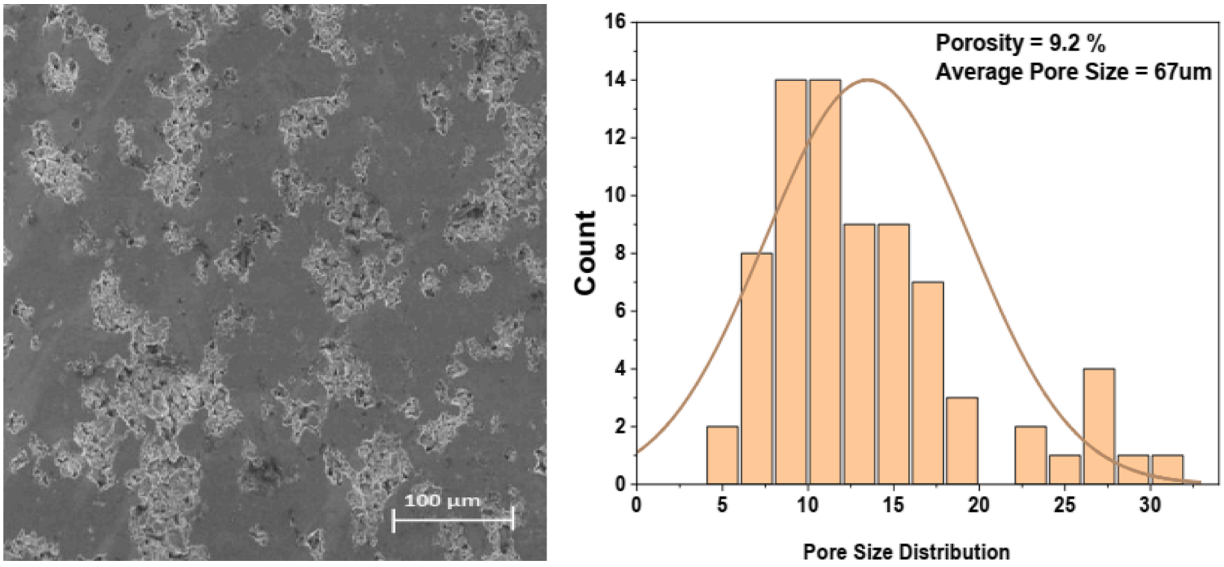

Fig. 12. SEM image and equivalent pore distribution plot.

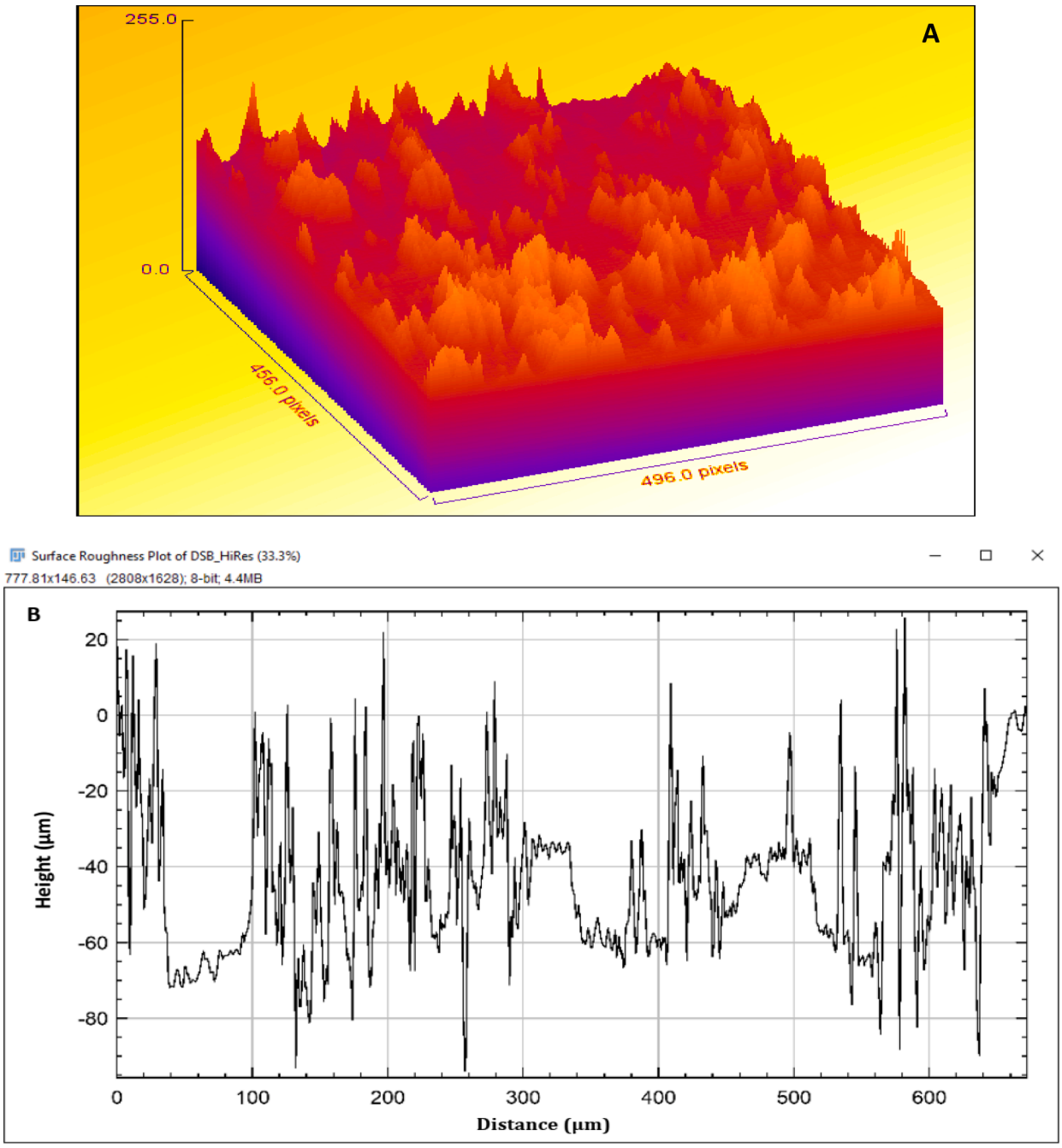

Fig. 13. Roughness surface plot (A) and profile plot (B) of DSB.

(26.11 MPam0.5).

CRediT authorship contribution statement

Ibrahim Hassan Kobe: Conceptualization, Investigation, Writing – original draft, Writing – review & editing, Resources. **Abdulrahman Asipital Salawu:** Conceptualization, Writing – original draft, Writing – review & editing, Resources. **Abolarin Mathew Sunday:** Conceptualization, Writing – original draft, Writing – review & editing, Resources. **Adedipe Oyewole:** Conceptualization, Writing – original draft, Writing – review & editing, Resources. **Okoro Gregory Uzoma:** Conceptualization, Writing – original draft, Writing – review & editing, Resources. **Peter Olorunleke Omoniyi:** Investigation, Writing – original draft, Writing – review & editing, Resources. **Tien-Chien Jen:** Writing – review & editing, Resources.

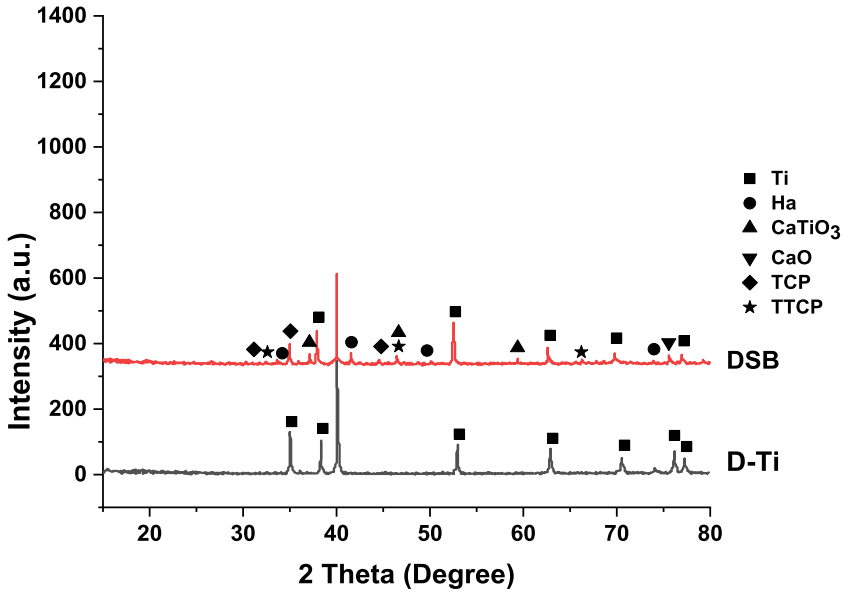

Fig. 14. XRD Results for DSB and equivalent densed Titanium (D-Ti) implant.

Declaration of competing interest

The authors declare that they have no known competing financial interests or personal relationships that could have appeared to influence the work reported in this paper.

References

[1] C. Pedneault, S. St George, B.A. Masri, Challenges to implementing total joint replacement programs in developing countries, Orthop. Clin. North Am. 51 (2020) 131–139, https://doi.org/10.1016/j.ocl.2019.11.001.
[2] G. Wei, M. Tan, S. Attarilar, J. Li, V.V. Uglov, B. Wang, J. Liu, L. Lu, L. Wang, An overview of surface modification, A way toward fabrication of nascent biomedical Ti–6Al–4V alloys, J. Mater. Res. Technol. 24 (2023) 5896–5921, https://doi.org/10.1016/j.jmrt.2023.04.046.
[3] S. Ali, A.M. Abdul Rani, Z. Baig, S.W. Ahmed, G. Hussain, K. Subramaniam, S. Hastuty, T.V.V.L.N. Rao, Biocompatibility and corrosion resistance of metallic biomaterials, Corros. Rev. 38 (2020) 381–402, https://doi.org/10.1515/corrrev-2020-0001.
[4] H.K. Ibrahim, M.S. Abolarin, A.S. Abdulrahman, P.O. Omoniyi, R.M. Mahamood, T.C. Jen, E.T. Akinlabi, Structural simulation of Ti–Ha–CaCO3 biocomposites using finite element analysis (FEA) for biomechanical stability of hip implant, Int. J. Interact. Des. Manuf. (2024) 1–14, https://doi.org/10.1007/s12008-024-01968-y.
[5] J.W. Pinto, G. Sujaykumar, R.M. Sushiledra, Effect of heat treatment on mechanical and wear characterization of coconut shell ash and E-glass Fiber reinforced aluminum hybrid composites, Am. J. Mater. Sci. 6 (2016) 15–19, https://doi.org/10.5923/c.materials.201601.03.
[6] P.S. Bains, S.S. Sidhu, H.S. Payal, Fabrication and machining of metal matrix composites: a review, Mater. Manuf. Process. 31 (2015) 553–573, https://doi.org/10.1080/10426914.2015.1025976.
[7] Q. Zhong, W. Li, X. Su, G. Li, Y. Zhou, S.C. Kundu, J. Yao, Y. Cai, Degradation pattern of porous CaCO3 and hydroxyapatite microspheres in vitro and in vivo for potential application in bone tissue engineering, Colloids Surf. B Biointerfaces 143 (2016) 56–63, https://doi.org/10.1016/j.colsurfb.2016.03.020.
[8] S. Ahmad, S.A. Alghamdi, A statistical approach to optimizing concrete mixture design, Sci. World J. 2014 (2014) 1–7, https://doi.org/10.1155/2014/561539.
[9] S. Debnath, M.N.L. Aishwarya, M.Iranajan Babu, Formulation by design: an approach to designing better drug delivery systems, Pharma Times 50 (2018) 9–14.
[10] N. Zarrinbakhsh, F.M. Defersha, A.K. Mohanty, M. Misra, A statistical approach to engineer a biocomposite formulation from biofuel coproduct with balanced properties, J. Appl. Polym. Sci. 131 (2014) 1–11, https://doi.org/10.1002/app.40443.
[11] N. Zarrinbakhsh, A.K. Mohanty, M. Misra, Formulation optimization of bioreinforced composites from polyolefins and dried distillers' grains using statistical methods, Compos. Part A Appl. Sci. Manuf. 119 (2019) 246–260, https://doi.org/10.1016/j.compositesa.2019.01.017.
[12] S.J.S. Chelladurai, M. K, A.P. Ray, M. Upadhyaya, V. Narasimharaj, G. S, Optimization of process parameters using response surface methodology: a review, Mater, Today Proc 37 (2021) 1301–1304, https://doi.org/10.1016/j.matpr.2020.06.466.
[13] V. Cannillo, L. Lusvarghi, A. Sola, Design of experiments (DOE) for the optimization of titania–hydroxyapatite functionally graded coatings, Int. J. Appl. Ceram. Technol. 6 (2009) 537–550, https://doi.org/10.1111/j.1744-7402.2008.02298.x.
[14] A. Tozar, İ.H. Karahan, Y. Yücel, Optimization of the electrophoretic deposition parameters for biocomposite hydroxyapatite/chitosan/collagen/h-BN coatings on Ti6Al4V biomedical implants, Metall. Mater. Trans. A 50 (2018) 1009–1020, https://doi.org/10.1007/s11661-018-5010-8.
[15] M. Elsayed, M. Ghazy, Y. Youssef, K. Essa, Optimization of SLM process parameters for Ti6Al4V medical implants, Rapid Prototyp. J. 25 (2018) 433–447, https://doi.org/10.1108/rpj-05-2018-0112.
[16] K. Nakai, K. Yamada, T. Nagata, Y. Saito, T. Nonomura, Effect of objective function on data-driven greedy sparse sensor optimization, IEEE Access 9 (2021) 46731–46743, https://doi.org/10.1109/access.2021.3067712.
[17] J. Djuris, D. Vasiljevic, S. Jokic, S. Ibric, Application of <scp>D</scp>-optimal experimental design method to optimize the formulation of <scp>O</scp>/<scp>W</scp>cosmetic emulsions, Int. J. Cosmet. Sci. 36 (2013) 79–87, https://doi.org/10.1111/ics.12099.
[18] E. Barua, P. Deb, S. Das Lala, A.B. Deoghare, Extraction of hydroxyapatite from bovine bone for sustainable development. Mater. Horizons From Nat. to Nanomater, Springer, Singapore, 2019, pp. 147–158, https://doi.org/10.1007/978-981-13-9977-0_10.
[19] H.M. Zakaria, Microstructural and corrosion behavior of Al/SiC metal matrix composites, Ain Shams Ehgineering J 5 (2014) 831–838, https://doi.org/10.1016/j.asej.2014.03.003.
[20] C. Prakash, S. Singh, S. Ramakrishna, G. Królczyk, C.H. Le, Microwave sintering of porous Ti–Nb-HA composite with high strength and enhanced bioactivity for implant applications, J. Alloys Compd. 824 (2020) 153774, https://doi.org/10.1016/j.jallcom.2020.153774.

[21] C. Srivabut, T. Ratanawilai, S. Hiziroglu, Response surface optimization and statistical analysis of composites made from calcium carbonate filler-added recycled polypropylene and rubberwood fiber, J. Thermoplast. Compos. Mater. 35 (2019) 391–415, https://doi.org/10.1177/0892705719889988.

[22] A. Nooraziah, V.J. Tiagrajah, A study on regression model using response surface methodology, Appl. Mech. Mater. 666 (2014) 235–239, https://doi.org/10.4028/www.scientific.net/amm.666.235.

[23] A. Arifin, A.B. Sulong, N. Muhamad, J. Syarif, M.I. Ramli, Material processing of hydroxyapatite and titanium alloy (HA/Ti) composite as implant materials using powder metallurgy: a review, Mater. Des. 55 (2014) 165–175, https://doi.org/10.1016/j.matdes.2013.09.045.

[24] S. Cummings, Microstructure and Mechanical properties of Titanium Alloys in Biomedical Application, University of Queensland Library, n.d. doi:10.14264/uql.2018.277.

[25] L.A. Shimp, Composites of hydroxyapatite and calcium carbonate and related methods of preparation and use, 2018.

[26] V. Saxena, V. Kumar, A. Rai, R. Yadav, U. Gupta, V.K. Singh, P.P. Manna, Optimization of the bio-mechanical properties of Ti–8Si–2Mn alloy by 1393B3 bioactive glass reinforcement, Mater. Res. Express 6 (2019) 75401, https://doi.org/10.1088/2053-1591/ab1280.

[27] V. Brailovski, P. Terriault, C. Simoneau, M. Dumas, B. Jetté, Development of a biomimetic metallic femoral stem: methodological approach, Mater. Sci. Forum 879 (2016) 1788–1793, https://doi.org/10.4028/www.scientific.net/msf.879.1788.

[28] C. Li, Z. Zhou, Charpy impact behavior of a novel stainless steel powder wire mesh composite porous plate, Materials (Basel) 14 (2021) 2924, https://doi.org/10.3390/ma14112924.

[29] J.A.S.A. Lawal, M.B.N.R.A. Lafia, A.O. Adedipe, Production and characterization of brake pad developed from coconut shell reinforcement material using central composite design, SN Appl. Sci. 1 (2019) 1–16, https://doi.org/10.1007/s42452-018-0084-x.

[30] M. Sadashiva, N.M. Siddeshkumar, J. Monica, M.R. Srinivasa, N. Santhosh, S. Praveenkumar, Hardness and impact strength characteristics of Al based hybrid composite FSW joints, Int. J. Veh. Struct. Syst. 14 (2022), https://doi.org/10.4273/ijvss.14.1.04.

[31] M. Suhandani, P. Puspitasari, J.A. Razak, Impact, hardness and fracture morphology of aluminium alloy (Al-Si) filled cobalt oxide nanoparticles at various stir casting temperatures, Malaysian J. Compos. Sci. Manuf. 5 (2021) 11–20, https://doi.org/10.37934/mjcsm.5.1.1120.

[32] W. Liu, C. Hu, L. Li, X. Zhang, L. Peng, Y. Qiao, Z. Yue, Experimental study on dynamic notch fracture toughness of V-notched rock specimens under impact loads, Eng. Fract. Mech. 259 (2022) 108109, https://doi.org/10.1016/j.engfracmech.2021.108109.

[33] H. Jelitto, G.A. Schneider, Fracture toughness of porous materials – Experimental methods and data, Data Br. 23 (2019) 103709, https://doi.org/10.1016/j.dib.2019.103709.

[34] I. Ćamagić, S.A. Sedmak, A. Sedmak, Z. Burzić, Influence of temperature on fracture toughness values in different regions of A-387 gr. B welded joint, Procedia Struct. Integr. 18 (2019) 205–213, https://doi.org/10.1016/j.prostr.2019.08.155.

[35] C. Homkhiew, T. Ratanawilai, W. Thongruang, The optimal formulation of recycled polypropylene/rubberwood flour composites from experiments with mixture design, Compos. Part B Eng. 56 (2014) 350–357, https://doi.org/10.1016/j.compositesb.2013.08.041.

[36] Z. Ban, P. Yuan, F. Yu, T. Peng, Q. Zhou, X. Hu, Machine learning predicts the functional composition of the protein corona and the cellular recognition of nanoparticles, Proc. Natl. Acad. Sci. 117 (2020) 10492–10499, https://doi.org/10.1073/pnas.1919755117.

[37] A. Al–bashir, M. Al-Dweri, A. Al–ghandoor, B. Hammad, W. Al–kouz, Analysis of effects of solar irradiance, cell temperature and wind speed on photovoltaic systems performance, Int. J. Energy Econ. Policy 10 (2020) 353–359, https://doi.org/10.32479/ijeep.8591.

[38] S.M. Moosavi, S. Ghassabian, Linearity of calibration curves for analytical methods: a review of criteria for assessment of method reliability. Calibration Valid. Anal. Methods - A Sampl. Curr. Approaches, InTech, 2018, https://doi.org/10.5772/intechopen.72932.

[39] H. Amadou, C. Beck, R. Mose, C. Vasile, A.-G. Sadowski, J.-B. Poulet, Analysis of the convective drying of residual sludge: from the experiment to the simulation. WIT Trans. Ecol. Environ. Vol 95, WIT Press, 2006, https://doi.org/10.2495/wp060451.

[40] E. Yılmaz, F. Kabataş, A. Gökçe, F. Fındık, Production and characterization of a bone-like porous Ti/Ti-hydroxyapatite functionally graded material, J. Mater. Eng. Perform. 29 (2020) 6455–6467, https://doi.org/10.1007/s11665-020-05165-2.

[41] F. Xie, J. Huang, H. Yang, X. He, Ti-10Mo/hydroxyapatite composites for orthopedic applications: microstructure, mechanical properties and biological activity, Mater. Today Commun. 29 (2021) 102887, https://doi.org/10.1016/j.mtcomm.2021.102887.

[42] C. Qian, F. Zhang, J. Sun, Fabrication of Ti/HA composite and functionally graded implant by three-dimensional printing, Biomed. Mater. Eng. 25 (2015) 127–136, https://doi.org/10.3233/bme-151263.

[43] S. Zhao, M. Arnold, R.L. Abel, J.P. Cobb, S. Ma, U. Hansen, O. Boughton, Standardizing compression testing for measuring the stiffness of Human bone, Bone Jt. Res. 7 (2018) 524–538, https://doi.org/10.1302/2046-3758.78.BJR-2018-0025.R1.

[44] I. Galan, B. Purgstaller, C. Grengg, B. Müller, M. Dietzel, Amorphous and crystalline CaCO3 phase transformation at high solid/liquid ratio – Insight to a novel binder system, J. Cryst. Growth 580 (2022) 126465, https://doi.org/10.1016/j.jcrysgro.2021.126465.

[45] C. Combes, B. Miao, R. Bareille, C. Rey, Preparation, physical–chemical characterisation and cytocompatibility of calcium carbonate cements, Biomaterials 27 (2006) 1945–1954, https://doi.org/10.1016/j.biomaterials.2005.09.026.

[46] M.F. Kunrath, C. Garaicoa-Pazmino, P.M. Giraldo-Osorno, A. Haj Mustafa, C. Dahlin, L. Larsson, F. Asa'ad, Implant surface modifications and their impact on osseointegration and peri-implant diseases through epigenetic changes: a scoping review, J. Periodontal Res. (2024) 1–20, https://doi.org/10.1111/jre.13273.

[47] H. Singh, Development of Titanium Based in Situ Composites By Powder Metallurgical route: Microstructure Evolution and Mechanical Properties, The University of Auckland, 2019.

[48] A.A. Abdel-Wahab, V. Silberschmidt, Dynamic properties of cortical bone tissue: impact tests and numerical study, Appl. Mech. Mater. 70 (2011) 387–392, https://doi.org/10.4028/www.scientific.net/amm.70.387.

[49] B. Beig, U. Liaqat, M.F.K. Niazi, I. Douna, M. Zahoor, M.B.K. Niazi, Current challenges and innovative developments in hydroxyapatite-based coatings on metallic materials for bone implantation: a review, Coatings 10 (2020) 1249, https://doi.org/10.3390/coatings10121249.

[50] M.-T. Choy, C.-Y. Tang, L. Chen, W.-C. Law, C.-P. Tsui, W.W. Lu, Microwave assisted-in situ synthesis of porous titanium/calcium phosphate composites and their in vitro apatite-forming capability, Compos. Part B Eng. 83 (2015) 50–57, https://doi.org/10.1016/j.compositesb.2015.08.046.

[51] H.K. Ibrahim, M.S. Abolarin, A.S. Abdulrahman, O. Adedipe, U.G. Okoro, Biomechanical and physical properties selection of Ti-ha-CaCO3 biocomposite prostheses for replacement of bone atrophy, Niger. J. Technol. Dev. 21 (2024) 42–52, https://doi.org/10.4314/njtd.v21i1.2174.

[52] J.L. Cabezas-Villa, L. Olmos, D. Bouvard, J. Lemus-Ruiz, O. Jiménez, Processing and properties of highly porous Ti6Al4V mimicking human bones, J. Mater. Res. 33 (2018) 650–661, https://doi.org/10.1557/jmr.2018.35.

[53] C. Prakash, H.K. Kansal, B.S. Pabla, S. Puri, Processing and characterization of novel biomimetic nanoporous bioceramic surface on β-Ti implant by powder mixed electric discharge machining, J. Mater. Eng. Perform. 24 (2015) 3622–3633, https://doi.org/10.1007/s11665-015-1619-6.

[54] M.U. Jurczyk, K. Jurczyk, A. Miklaszewski, M. Jurczyk, Nanostructured titanium-45S5 bioglass scaffold composites for medical applications, Mater. Des. 32 (2011) 4882–4889, https://doi.org/10.1016/j.matdes.2011.06.005.